Catena 134 (2015) 30–40

Contents lists available at ScienceDirect

Catena

journal homepage: www.elsevier.com/locate/catena

The Southern Westerlies in Central Chile during the two last glacial cycles as documented by coastal aeolian sand deposits and intercalating palaeosols

Heinz Veit [a,*], Frank Preusser [b,1], Mareike Trauerstein [a]

[a] Institute of Geography, University of Bern, Hallerstrasse 12, 3012 Bern, Switzerland
[b] Department of Physical Geography and Quaternary Geology, Stockholm University, 10691 Stockholm, Sweden

ARTICLE INFO

Article history:
Received 21 May 2014
Received in revised form 11 October 2014
Accepted 3 November 2014
Available online 28 November 2014

Keywords:
Quaternary
Southern Westerly Winds
Chile
Dunes
Paleosols
Luminescence dating

ABSTRACT

Changes in the position and intensity of the Southern Westerly Winds (SWW) and related causal processes during the Quaternary are controversial and not well understood. Here, we present a record from continental Central Chile, based on coastal aeolian sand and dunes with intercalated palaeosols, reaching back 190 ka in time. Sixteen samples for luminescence dating and additional samples for geochemical procedures were analysed from three locations in the "Norte Chico" (La Serena, Los Vilos, Las Ventanas). Besides the recent Bw-horizons, four palaeosols (Btb1, Btb2, Btb3, Btb4) are identified. They formed in periods with stable surface conditions and a relatively dense vegetation cover, whereas sand accumulation reflects increased aeolian activity under dry conditions and, in parts, glacial sea level lowering. Three of these soils are well bracketed by luminescence data to <14 ka (Bw), 59–47 ka (Btb4) and 135–125 ka (Btb2). The formation of Btb1 and Btb3 tentatively occurred at 190–160 ka and 107–95 ka. Btb-horizons are interpreted to reflect wetter conditions than modern ones (Bw-horizons). Since the only way to bring wetter conditions to the coastal area of the Norte Chico are the SWW, the documented changes should reflect changes in paleo atmospheric circulation. The more humid periods appear to show a periodicity, dominated by the obliquity cycle. Increased Antarctic sea-ice during austral winter combined with a weak South Pacific Anticyclone at subtropical latitudes, seem to have favoured winter incursions of humid air masses from the Westerlies.

1. Introduction

The Southern Westerly Winds (SWW), along with the Antarctic Circumpolar Current (ACC), are an important component of the global climate system. They regulate meridional heat flux and likely also the concentration of atmospheric carbon dioxide (Marchant et al., 2007; Rojas et al., 2009; Hodgson and Sime, 2010; Moreno et al., 2010). Little is known about the variability of these systems over longer time scales, and this topic has led to controversial discussions over the past decades (e.g., Kohfeld et al., 2013). Most studies have focused on changes during the global Last Glacial Maximum (LGM), leaving it unclear whether northward or southward shifts of the SWW occurred in the past, or if there were even any shifts at all.

Based on most palynological studies, a northward shift of the SWW during the LGM and a corresponding southward shift during the Early Holocene has been concluded (e.g. Heusser, 1989; Villagrán, 1990; Villagrán and Armesto, 1993; Villa-Martínez et al., 2003; Villagrán et al., 2004; Mayr et al., 2007). However, Markgraf (1989), and Markgraf et al. (1992) instead postulated a southward movement during the LGM. Limnological (e.g. Jenny et al., 2002, 2003; Valero-Garcés et al., 2005; Gilli et al., 2005), pedological (e.g. Veit, 1996) and marine (e.g. Lamy et al., 2001, 2002; Stuut and Lamy, 2004; Stuut et al., 2006; Toggweiler et al., 2006; Kaiser et al., 2008) studies point to a northward shift of the SWW during the LGM and a southward retreat during the Holocene which support the palynological assumptions. Glacier advances, in Central Chile, however, predate the global LGM (Zech et al., 2006, 2008, 2011), indicating an earlier northward shift of the SWW and a dry LGM. Results from modelling studies are controversial, including southward shifts during the LGM (Valdes, 2000; Wyrwoll et al., 2000; Wainer et al., 2005), northward shifts (Caviedes, 1990) and no shifts at all with only intensity changes (Kull et al., 2002; Rojas et al., 2009).

In this paper, a palaeoecological reconstruction of the Norte Chico (Fig. 1) reaching back 190 ka will be presented, based on alternating periods of aeolian sand accumulation and soil development along the semiarid coast of Central Chile. The sediments and soil horizons have been characterised during field work and laboratory analyses, and the

* Corresponding author at: Institute of Geography, University of Bern, Hallerstrasse 12, 3012 Bern, Schweiz.
E-mail addresses: veit@giub.unibe.ch (H. Veit), frank.preusser@natgeo.su.se (F. Preusser), mareike.trauerstein@giub.unibe.ch (M. Trauerstein).
[1] Present address: Institute of Earth and Environmental Sciences-Geology, University of Freiburg, Albert Strasse 23-B, 79104 Freiburg, Germany.

http://dx.doi.org/10.1016/j.catena.2014.11.002
0341-8162/

Fig. 1. Location of the study areas La Serena, Los Vilos and Las Ventanas.

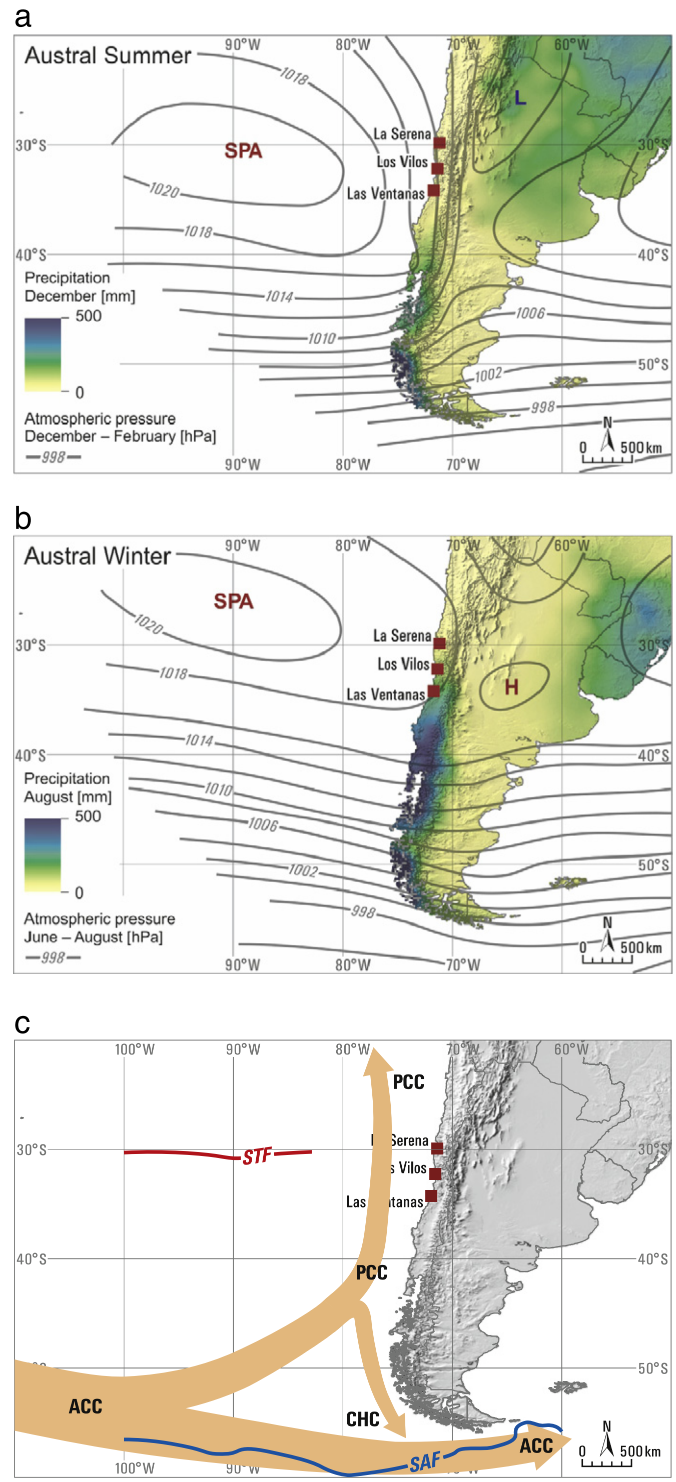

Fig. 2. Major climatic and marine features in the SE-Pacific; a) + b) seasonal precipitation and position of the SPA (after Hijmans et al., 2005; Saavedra et al., 2010), c) ACC and marine frontal systems (Ho et al., 2012). SPA = South Pacific Anticyclone; ACC = Antarctic Circumpolar Current; PCC = Peru–Chile Current; CHC = Cape Horn Current; STF = Subtropical Front; SAF = Subantarctic Front.

age of aeolian sand deposition has been determined using luminescence dating. As the latter is not a straight forward process, we put a major focus on investigating the reliability of the dating results. The results presented here are examined in the context of evidence from marine deposits and implications for past dynamics of the SWW/ACC system are discussed.

2. Regional setting

The “Norte Chico”, between Valparaiso and La Serena, is a semiarid region with annual precipitation between 400–80 mm, with a clear trend of decreasing precipitation towards the north (Fig. 2). Accordingly, vegetation shifts from sclerophyllous woodland in the south to xerophytic thorn shrub, with a sharp transition to the Atacama Desert north of 28°S (Armesto et al., 2007). Precipitation is entirely linked to moisture-bearing SWW during their northernmost position in austral winter, which itself is controlled by the latitudinal position and strength of the South Pacific Anticyclone (SPA) as well as the extent of sea-ice around Antarctica (Stuut and Lamy, 2004; Ho et al., 2012; Fig. 2). A weak SPA in a northerly position allows the westerly storm tracks to penetrate further north. Vice versa, a strong SPA in a relatively southerly position leads to a blocking situation and dry winters in Central Chile. This geographical position makes the Norte Chico a very sensitive region for changes in the position and intensity of the SWW and SPA. A major component of the inter-annual variability in precipitation is linked to the El Niño Southern Oscillation (ENSO; Aceituno, 1988; Ruttland and Fuenzalida, 1991; Simmonds and Jacka, 1995; Cerveny, 1998; Karoly, 1989; Lu et al., 2010). A weakening of the SPA during El Niño conditions leads to increased precipitation through stronger influence of the SWW in mediterranean Chile, whereas La Niña episodes are characterised by dry conditions and a strengthening of the SPA.

The modern wind regime along the coast is characterised by predominantly southerly to westerly winds (Saavedra et al., 2010). Wind speed is highest during austral summer, reaching ca. 6.5-10 m s^{-1} in the monthly mean (Garreaud and Falvey, 2009; Rahn and Garreaud, 2013), which is sufficient for transporting fine to medium sand. The prevailing winds are reflected by the activity of modern dunes, which are mostly restricted to areas north of river mouths with sufficient sand supply. Inactive and fossil dunes are found far more widespread than modern ones along the coast of the Norte Chico, typically situated on top of Quaternary marine terraces (Herm and Paskoff, 1967; Paskoff, 1970; Radtke, 1989).

3. Methods

3.1. Characterisation of soils and sediments

Sediments and soil/palaeosol horizons were described during field work according to their visible characteristics (stratification, grain size, colour). Thin sections were investigated to trace clay illuviation of the Bt-horizons. Sediment and soil samples were taken to analyse grain size, clay minerals, heavy minerals, pH, pedogenic iron, and cation exchange capacity (CEC) following standard procedures. Prior to grain size measurement sesquioxides were removed from the samples by adding 0.3 M sodium citrate-solution, 1 M sodium carbonate-solution and sodium dithionite. Organic matter was removed by oxidation with 30% H_2O_2. A solution of sodium hexametaphosphate with sodium carbonate was added as a dispergent agent. The sand fractions were determined by wet sieving (dispersion with Na_2CO_3). The silt fractions and the clay fraction were analysed using the Micromeritics SediGraph 5100. The soil samples did not show reaction to HCl in the field, therefore, $CaCO_3$ was not analysed in the lab. The pH was measured with a glass electrode in 0.01 M $CaCl_2$ in a proportion of 1:2.5 (soil:solution). Total pedogenic iron (Fe_d) and amorphous pedogenic iron (Fe_o) were extracted with dithionite and oxalate (Mehra and Jackson, 1960; Schwertmann, 1964) and measured with a photometer (Merck Pharo100). Clay minerals were identified by X-ray diffraction using orientated samples with three pre-treatments: air-dry, saturated with ethylene glycol, and heated to 550 °C. For heavy mineral analyses, samples were sieved to separate the 100–200 μm fraction. This fraction was pre-treated with 10% HCl (100 °C) to remove coatings of iron oxides and clay minerals. Heavy minerals were separated using heavy liquid (solution of sodiumpolytungstenate in water, 2.9 g/cm^3), embedded into synthetic resin and determined using a petrographic microscope. For CEC 5 g of soil were treated with 100 ml ammonium nitrat (NH_4NO_3) for one hour and measured using atomic absorption spectroscopy (AAS).

3.2. Luminescence dating

Altogether, 16 samples for luminescence dating were taken from the base and the top of the different generations of aeolian sand deposition. Soil ages were estimated to lie between the age of the older parent material and the covering sands. For equivalent dose (D_e) determination, samples were dry sieved to separate the 150–200 μm grain size fraction, followed by HCl and H_2O_2 treatment. A quartz and feldspar fraction was extracted using heavy liquids (2.70 g cm^{-3}, 2.58 g cm^{-3}), and quartz was subsequently etched in 40% HF for 1 h. As the samples were taken from aeolian deposits, the material was assumed to be well bleached and the use of large aliquots (4 mm) for all subsequent luminescence measurements was considered appropriate. Luminescence measurements were carried out on a Risø DA-20 TL/OSL reader fitted with an internal $^{90}Sr/^{90}Y$ beta-source. Quartz signals were detected through a Hoya U340 detection filter, and feldspar signals with a combination of a Schott BG-39 and a 410 nm interference glass filter.

Initial test measurements on quartz revealed that its optically stimulated luminescence (OSL) signal is very dim and dominated by an unstable signal component that makes it unsuitable for dating. This appears to be a common problem for sediments from the western escarpment of the Andes (Steffen et al., 2009; Trauerstein et al., 2014). The infrared stimulated luminescence (IRSL) signal of potassium-rich feldspar offers an alternative, but is problematic due to possible anomalous fading of the IRSL signal – an athermal signal loss over time which leads to age underestimation (Wintle, 1973; Spooner, 1994). D_e determination using the IRSL signal of feldspar was carried out on 5–7 aliquots per sample applying a single-aliquot regenerative-dose (SAR) protocol. The same preheat of 250 °C for 60 seconds was applied before the regeneration dose and test dose measurement (Blair et al., 2005) and the signal stimulation was performed at 50 °C (termed IR50 from this point). To detect possible fading of the IR50 signal, delayed measurements with different storage times between irradiation and IR50 measurement (Auclair et al., 2003) were carried out on 6 samples (VEC02,03,06,10,11,12,14). They revealed similar fading rates between 3.5 and 4.1% per decade for all samples. These results demonstrate that the IR50 signal is apparently affected by fading and that the resulting IR50 ages very likely underestimate the true depositional age. The most commonly adopted fading correction method of Huntley and Lamothe (2001) claims to be valid only in the low-dose region of the dose response curve, which is to say only for samples of young age (<50 ka). The corrected IR50 ages are presented in Table 1.

A recently developed strategy to overcome the fading problem is to focus on measuring IRSL at elevated temperature after IRSL readout at 50 °C (post-IR IRSL; Thomsen et al., 2008; Buylaert et al., 2009). This signal appears to exhibit little or no fading and therefore eliminates the need for age corrections. Nonetheless, the possibility of residual doses originating from hard-to-bleach or thermal transfer of non-bleachable charge has to be taken into account. In this study, D_e determination using the post-IR IRSL signal was performed on 7–9 aliquots per sample following the protocol of Buylaert et al. (2009). This protocol includes preheating at 250 °C for 60 s, a first IRSL readout at 50 °C followed by IRSL measurement at 225 °C (termed PostIR225 from this point). Residual doses were determined for all samples after bleaching the sample material for 72 h with a Sunlux Ambience UV lamp. The residual dose measurements revealed residual doses between 4 and 20 Gy (Fig. 3, Table 1). Dose recovery tests were performed on three samples (VEC03, VEC06 and VEC12), after using the same bleaching procedure as for the residual dose measurements and with a given dose similar to the determined PostIR225 D_e (190, 430 and 80 Gy, respectively). The dose recovery ratio for the three samples was 1.09 ± 0.4, 1.06 ± 0.3 and 1.06 ± 0.03, respectively. The slight overestimation observed in these tests could be explained by the effect of residuals.

Plotting the measured PostIR225 residual doses against the postIR225 D_e values reveals a positive correlation (Fig. 3). A tendency for residual doses to grow with D_e could also be observed by other authors (Sohbati et al., 2011; Buylaert et al., 2012; Preusser et al., 2014). It is unlikely that the residual dose prior to deposition is related to the subsequent burial dose and therefore the measured residuals here might reflect a hard-to-bleach component of the signal rather than an actual residual that has to be subtracted. As the measured residuals account for only 3–8% of the determined D_e values, subtracting them would have a negligible effect on the interpretation of ages in the present context.

The comparison between the fading corrected IR50 and the postIR225 shows that they are proportional in the lower age range (up to ca. 60 ka), whereas in the upper age range the fading corrected IR50 ages tend to underestimate the PostIR225 ages (Fig. 4). This underestimation could be explained by the limitations of the fading correction used as it is restricted to samples that are within the linear part of signal growth, which for our samples applies to those aged <50 ka. Therefore the postIR225 ages are considered more reliable and are further used in the discussion.

The concentration of dose rate relevant elements was determined using high-resolution low-level gamma spectrometry (cf. Preusser and

Table 1
Sample depth, concentration of dose rate relevant elements (K, Th, U), dose rates (D), number of aliquots used for D_e determination for IR50/PostIR225, results of D_e determination and corresponding ages for IR50 and PostIR225, respectively. Fading correction after Huntley and Lamothe (2001) using an average g-value of 3.80 ± 0.25%/decade for all samples.

Sample	Depth (cm)	K (%)	Th (ppm)	U (ppm)	D (Gy ka^{-1})	n	IR50 D_e (Gy)	PostIR225 D_e (Gy)	PostIR225 residual (Gy)	IR50 age (ka)	IR50 age corrected (ka)	PostIR22 age (ka)
VEC1	65	2.36 ± 0.05	7.46 ± 0.24	1.66 ± 0.04	3.99 ± 0.14	5/7	42 ± 3	57 ± 4	4 ± 0	11 ± 1	15 ± 1	14 ± 1
VEC2	110	2.31 ± 0.05	7.38 ± 0.17	1.66 ± 0.11	3.92 ± 0.15	5/9	146 ± 3	187 ± 4	7 ± 1	37 ± 2	52 ± 3	48 ± 2
VEC3	160	2.32 ± 0.05	7.99 ± 0.11	1.53 ± 0.03	3.89 ± 0.12	7/7	189 ± 10	233 ± 7	11 ± 1	48 ± 3	67 ± 5	60 ± 3
VEC4	220	2.29 ± 0.05	6.31 ± 0.22	1.35 ± 0.08	3.73 ± 0.13	5/9	236 ± 12	381 ± 18	10 ± 0	63 ± 4	88 ± 6	102 ± 6
VEC5	300	2.32 ± 0.05	7.95 ± 0.28	1.61 ± 0.03	3.78 ± 0.11	5/7	302 ± 18	474 ± 24	13 ± 1	80 ± 5	111 ± 8	125 ± 7
VEC6	400	2.18 ± 0.05	9.66 ± 0.37	1.60 ± 0.05	3.86 ± 0.14	5/9	364 ± 30	522 ± 24	15 ± 0	94 ± 8	131 ± 12	135 ± 8
VEC7	600	2.16 ± 0.04	10.31 ± 0.30	1.65 ± 0.04	3.92 ± 0.16	5/7	402 ± 34	763 ± 37	20 ± 3	103 ± 10	143 ± 14	195 ± 12
VEC8	300	1.68 ± 0.03	7.35 ± 0.17	1.65 ± 0.05[d]	3.26 ± 0.11	5/7	262 ± 5	348 ± 33	18 ± 2	80 ± 3	112 ± 5	107 ± 11
VEC9	600	1.77 ± 0.04	6.93 ± 0.11	1.71 ± 0.04	3.29 ± 0.10	7/7	263 ± 14	412 ± 41	15 ± 1	80 ± 5	111 ± 7	125 ± 13
VEC10	900	1.61 ± 0.03	6.98 ± 0.26	1.68 ± 0.01	3.11 ± 0.11	7/9	327 ± 15	497 ± 19	16 ± 1	105 ± 6	147 ± 9	160 ± 8
VEC11	1000	1.57 ± 0.03	6.15 ± 0.15	1.38 ± 0.04	2.92 ± 0.11	7/7	362 ± 14	560 ± 27	18 ± 1	124 ± 7	173 ± 10	192 ± 12
VEC12	400	2.08 ± 0.04	5.33 ± 0.07	1.34 ± 0.06	3.40 ± 0.12	5/7	63 ± 2	74 ± 3	6 ± 1	18 ± 1	25 ± 1	22 ± 1
VEC13	200	1.94 ± 0.04	5.52 ± 0.12	1.35 ± 0.07	3.30 ± 0.13	5/9	77 ± 3	92 ± 4	6 ± 0	23 ± 1	32 ± 2	28 ± 2
VEC14	330	1.41 ± 0.03	7.47 ± 0.21	1.62 ± 0.04	3.01 ± 0.11	5/9	286 ± 9	377 ± 12	13 ± 1	95 ± 5	133 ± 7	125 ± 6
VEC15	310	1.91 ± 0.04	5.73 ± 0.25	1.35 ± 0.05	3.30 ± 0.12	5/7	115 ± 3	159 ± 10	12 ± 1	35 ± 2	49 ± 2	48 ± 3
VEC16	110	1.72 ± 0.04	6.25 ± 0.18	1.63 ± 0.03	3.28 ± 0.12	5/7	53 ± 3	71 ± 3	5 ± 1	16 ± 1	22 ± 2	22 ± 1

Kasper, 2001). Luminescence ages have been calculated using ADELE software (Kulig, 2005) using present day depth for the calculation of cosmic dose rate, assuming an internal K-content of feldspar of 12.5 ± 0.5% (Huntley and Baril, 1997) and an a-value of 0.07 ± 0.02. For the calculation of dose rate, it was assumed that the average sediment moisture since was between 0 and 6%. The dosimetric data is summarised in Table 1.

4. Profile descriptions and palaeopedological analyses

The investigated profiles "La Serena", "Los Vilos", and "Las Ventanas" are situated between 30–33°S (Fig. 1). In all three sections, several generations of aeolian deposition and intercalated palaeosols are present. Modern surfaces are stable under natural conditions and covered by a xerophytic thorn shrub. The modern topsoil is always weakly developed, with soft Ah- or Bw-horizons. In contrast, the indurated palaeosols show intense clay illuviation (Btb-horizons; Figs. 5–7). All Btb-horizons have a similar morphological development. According to their ages they are named Btb1 to Btb4 (Figs. 8 and 9).

4.1. La Serena, Quebrada Peñuelas (29°55′S)

The studied section at La Serena is situated at the transition from the highest marine terrace, known as Serena-I (at about 120 m above sea-level, about 4 km from the coast and probably Plio-/Pleistocene in age (Herm and Paskoff, 1967; Paskoff, 1970; Radtke, 1989)), down to the Herradura-I terrace (MIS 9 or MIS 11; Radtke, 1989). In the so-called "Garganta del Diablo", close to Tierras Blancas (Quebrada Peñuelas), several palaeosols intercalating aeolian deposits were exposed in a gully (Fig. 5). The modern soil is characterised by a weakly developed, light brown Bw-horizon down to 0.4–0.5 m (Fig. 5c). The parent material consists of an aeolian sand cover, with a fairly constant thickness of 1–1.5 m. This sand overlies the surface of an older aeolian deposit, indurated by a reddish-brown palaeosol. It is a 1–2 m thick, strongly cemented Btb-horizon (Btb4) with clay cutans, clearly visible in the field and in the thin sections (Fig. 5d). As a special feature, this Btb-horizon shows impressive dry cracks, filled with the younger unconsolidated aeolian sand. In the upper part of the Btb, these cracks open to 10–15 cm, reaching down to 1 m or even more. The distance of one dry crack to another is about 1–5 m, forming polygons at the surface (Fig. 5e). The massive Btb grades into a laminated horizon down to 3.5 m, where the next aeolian unit is indicated by annother Btb-horizon (Btb2). The texture of the sediments is dominated by middle and fine sand, with minor amounts of silt (Table 2). The clay content of the unweathered aeolian material is <1%, reaching 11–25% in the Btb-horizons. Main components of the heavy minerals are Epidote and Amphiboles, reflecting the granitic environment of the coastal cordillera. Fe_d values are highest in the Btbs and lower in the Bw-horizons. Fe_o values are generally very low and pH-values show neutral conditions. Aeolian sands do not show reaction to 10% HCl. Parts of the CEC are characterised by Na^+-contents of up to 13%, which might locally influence dispergation of the soil and favour clay illuviation.

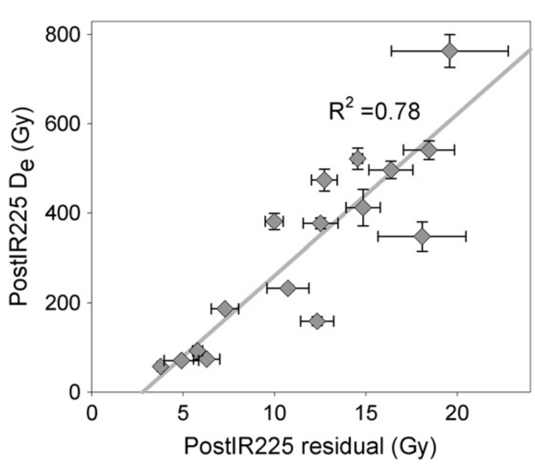

Fig. 3. PostIR225 residual dose plotted against the PostIR225 D_e value of each sample.

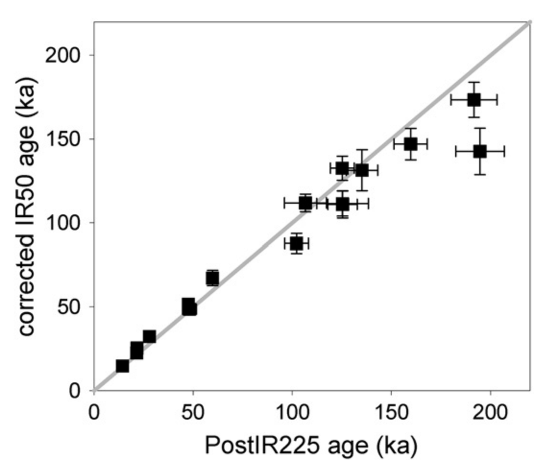

Fig. 4. Luminescence ages derived from the PostIR225 plotted against those derived from the IR50 corrected for fading.

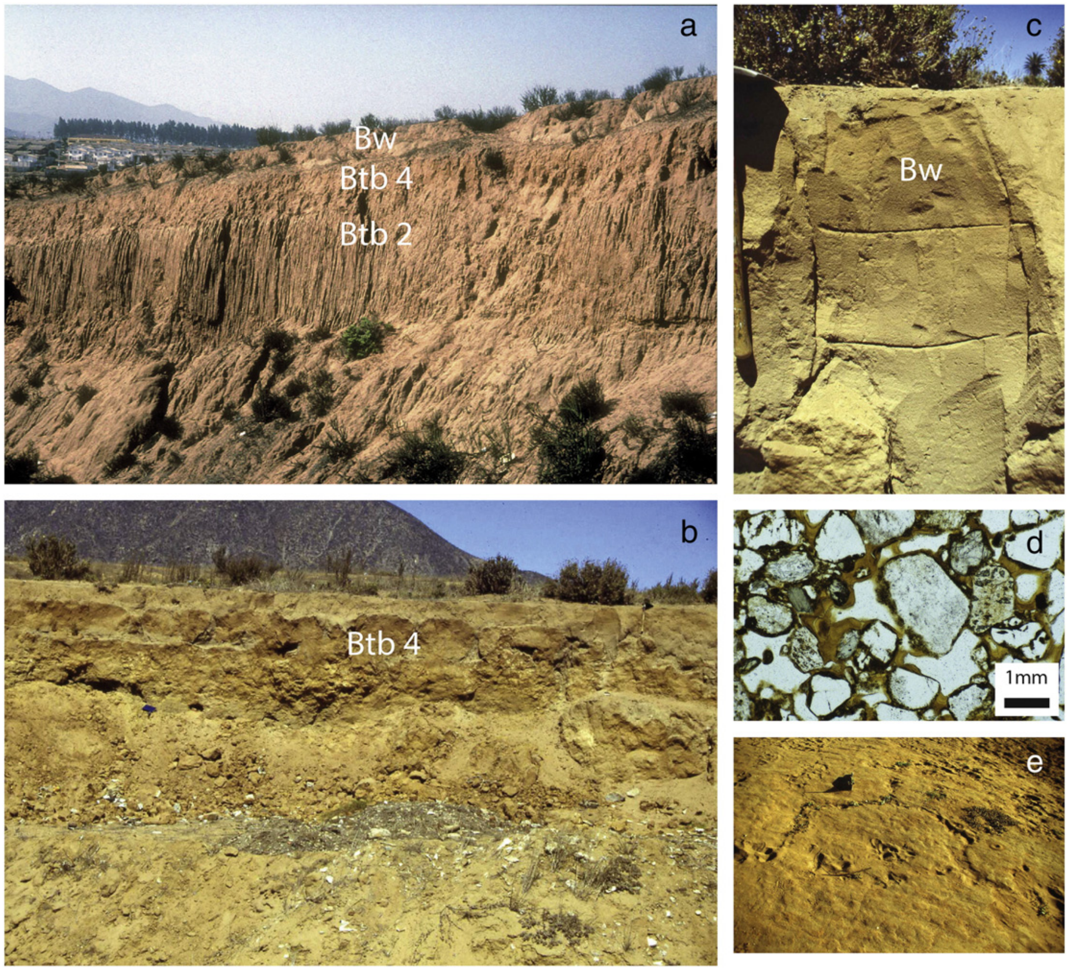

Fig. 5. Profile La Serena; a) overview with three dune generations and corresponding soils (Bw, Btb4, Btb2); b) Btb4-horizon with dry cracks and overlying LGM-dune; c) weakly developed modern Bw-horizon; d) thin section of fBt4-horizon with clay cutans; e) dry crack polygons on the palaeosurface of the Btb4-horizon.

4.2. Los Vilos (31°51′S)

The profile at Los Vilos is directly situated at both flanks of the Panamericana, at the end of the bay north of Los Vilos (Fig. 6). Aeolian sand overlies marine gravels of the Herradura-I terrace. The succession of aeolian deposits and palaeosols appears very similar to the profile at La Serena. Weak Ah- and Bw-horizons on the youngest dune stand in contrast with the reddish-brown Btb-horizon between 3.5–5.0 m (Btb3). The next Btb (Btb1) follows below 7.0 m. As in La Serena, the texture of the aeolian material is dominated by medium and fine sand, with small amounts of silt. In contrast to La Serena, the sands of the Btb-horizons contain small stones from the local basement, indicating postsedimentary local hillwash processes. Mineralogy, pH and pedogenic iron contents are similar to La Serena and Los Vilos (Table 2).

4.3. Las Ventanas (32°46′S)

Between La Laguna and Quintero the marine H-I terrace is widely covered by inactive dunes. The studied profile at Las Ventanas is directly north of the power plant, at the eastern flank of the Panamericana. As in La Serena and Los Vilos, it shows a weak Bw-horizon in the upper part and a strongly developed Btb-horizon at 4.5 m depth (Btb3, Fig. 7). In contrast to the other two profiles, the Bw-horizon is covered by even younger aeolian sands. These sands show only minor soil development (Ah-horizon).

5. Chronological framework

From field evidence alone, it is obvious that all studied sections overlie and are therefore younger than, the marine Herradura-I terrace, which is assigned based on ESR dating to MIS 9 or MIS 11 (Radtke, 1989). Therefore, the sequences must represent at least the last two glacial cycles. The profile at La Serena shows consistent ages between 195 $\pm$ 12 ka at the base and 14 $\pm$ 1 ka close to the top (Fig. 8). The oldest phase of aeolian deposition stopped shortly after 135 $\pm$ 8 ka, after which a strong palaeosol (Btb2) developed. It was covered by sand prior to 125 $\pm$ 7 ka, when the next generation of aeolian accumulation began building up. Therefore, soil formation occurred at ca. 135–125 ka. The accumulation of the younger aeolian unit came to an end after 60 $\pm$ 3 ka and the next Bt-horizon (Btb4) subsequently developed. This soil was covered by sand prior to 48 $\pm$ 2 ka. Soil formation occurred in the intermediate time interval at ca. 59–47 ka. The accumulation of the youngest aeolian sand continued at least until 14 $\pm$ 1 ka. The Bw-horizon developed during the Late Pleistocene/Holocene.

At Los Vilos, the interpretation of the luminescence data is not as straightforward. Similar to La Serena, ages range from 192 $\pm$ 12 ka at the bottom to 22 $\pm$ 1 ka at the top. The oldest palaeosol (Btb1) developed after 191 $\pm$ 12 ka and was covered by sand prior to 160 $\pm$ 8 ka. The overlying sands accumulated until 107 $\pm$ 11 ka. Soil formation of the Btb3 is interpreted to have occurred shortly afterwards. The next phase of sand accumulation only occurred much later during the LGM. Soil formation of the Btb3 is interpreted to have occurred close to

Fig. 6. Profile Los Vilos; a) Google image, showing white modern dunes north of Estero Conchalí (view northwards) and position of the studied profile (white star); b) view from the studied profile with brown sands towards the south, over the modern white dunes to Estero Conchalí; c) detail of the profile, LGM-dune, overlying reddish-brown palaeosol (Btb3-horizon, below spate).

106–90 (?) ka, whereas the younger age is only an estimate, assuming that, as in La Serena (Btb2, Btb4), Bt-formation took ca. 10–15 ka. The youngest dune sands accumulated during the LGM followed by development of a Bw-horizon during the Lateglacial/Holocene, after 22 ± 2 ka.

At Las Ventanas, luminescence ages range from 125 ± 6 ka at the bottom to 22 ± 1 ka at the top. Compared to Los Vilos, the accumulation of the older dune sand probably did not stop at 125 ± 6 ka but instead at 107 ± 11 ka. At Los Vilos the luminescence sample was taken closer to the palaeosurface, yielding a more accurate date for the end of the corresponding sand accumulation. Therefore, the Btb-horizon at Las Ventanas is interpreted to stratigraphically reflect the same Btb3 as in Los Vilos. After a hiatus, the basal part of the younger sands accumulated at 48 ± 4 ka and continued accumulating until 22 ± 1 ka. In contrast to Los Vilos and La Serena, the Bw-horizon is covered by even younger sand, which show only minor soil formation (Ah-horizon). Due to the

Fig. 7. Profile Las Ventanas; weak Bw-horizon in LGM-dune, overlying thick Btb3-horizon.

colluvial character of this sand, no luminescence samples were taken. The very weak soil formation may indicate a very recent, human induced accumulation of the uppermost cover sands.

At all three locations, the development of the weak Bw-horizon is indicated to have occurred after the accumulation of sands had come to an end at about 14 ± 1 ka, 22 ± 1 ka and 22 ± 1 ka (Fig. 7). Assuming the youngest age to be the most probable, the Bw-horizon developed during the Lateglacial/Holocene.

Besides the recent Bw-horizons, four palaeosols (Btb1–4) may be distinguished. Neither all accumulation periods nor all soil forming periods are reflected in each profile. There are clear discontinuities, which is not astonishing for a terrestrial archive. The clearest chronology is for La Serena, where Btb2 and Btb4 are well bracketed by luminescence ages. Btb1 is only exposed at Los Vilos, and Btb2 appears only at La Serena. The lack of Btb1 at La Serena as well as the lack of Btb2 at Los Vilos could indicate an erosional hiatus or ongoing sand accumulation due to, for example, high wind speeds and the close proximity of the beach. Due to local environmental differences, not all locations necessarily reacted with comparable sensitivity. Btb3 is present at Los Vilos and Las Ventanas, whereas Btb4 is only present at La Serena. MIS 3 and MIS 4 sands are lacking at Los Vilos and Las Ventanas, but present at La Serena. Sand from the pre-LGM to Lateglacial times (48–14 ka) is present at all three locations.

6. Discussion

Accumulation of aeolian sands and soil evolution seem to follow a periodic pattern during the last 190 ka (Fig. 9). Active coastal dunes in the Norte Chico are typically restricted to relatively small areas, frequently north of a river mouth, were there is enough nonvegetated sandy material available (Fig. 6a). Due to the dominant rocky cliff-coast in the Norte Chico, source material for aeolian transport and dune formation today is scarce. Vegetated and inactive dunes are far more widespread and characterise many parts of the coast between Valparaiso and La Serena. The xerophytic thorn shrubs have allowed the formation of Ah- and Bw-horizons on stabilised dunes. The Bw-horizons seem to represent the modern – Late Glacial to Holocene – semiarid conditions. The low Fe_o values are typical for desert soils, due to the lack of organic material and rapid crystallisation of the iron oxides (Blume, 1985). Clay formation and infiltration is close to zero (Table 2). Illites characterize 100% of the clay minerals. The development of the Btb-horizons is in sharp contrast with the Bw-horizons. Clay formation and infiltration resulting in clay enrichments of 11–25% (Table 2), clay cutans (Fig. 5d), high amounts of interlayered clay minerals (Table 2), thicknesses of the Btb-horizons up to more than 2 m with clay lamellae

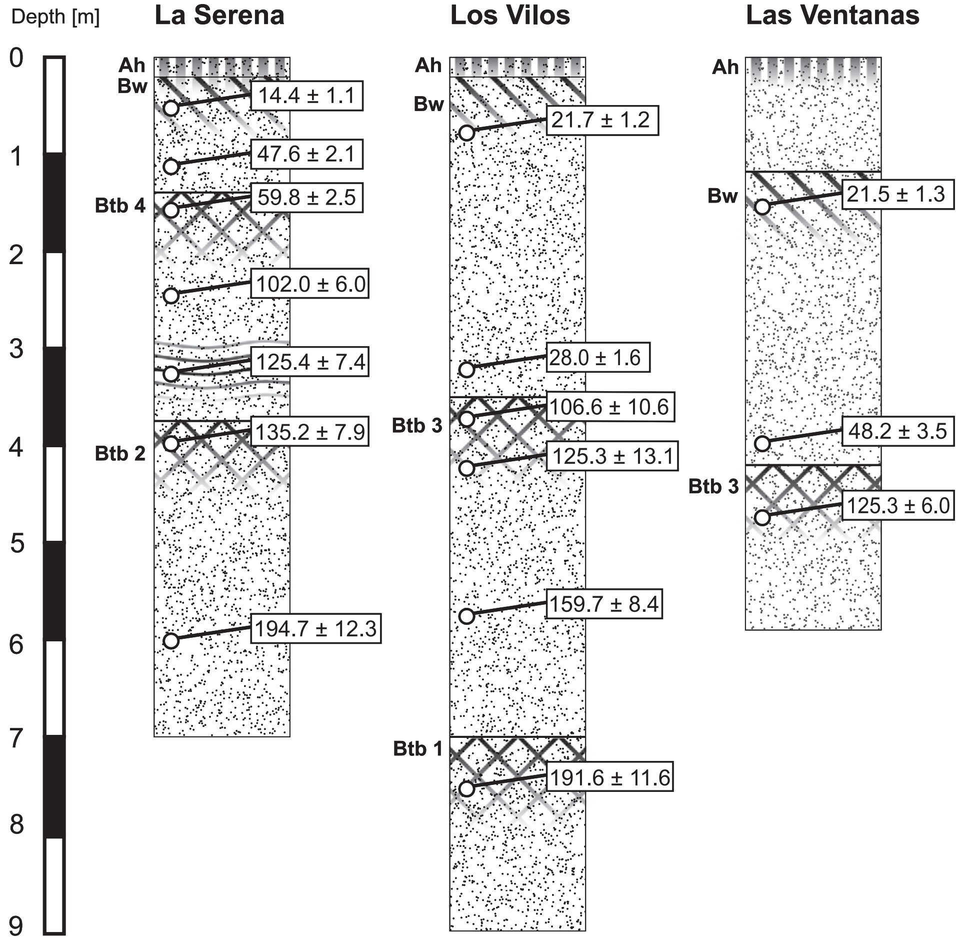

Fig. 8. Schematic sketch of the profiles La Serena, Los Vilos and Las Ventanas with luminescence ages (postIR225).

reaching further down, altogether points to wetter than modern conditions. Where the Bt-horizons are not overlain by aeolian sand or other younger cover-beds, they form the surface soils. Their colour and well developed structure has already been used for classifying them as Pleistocene palaeosols, reflecting wetter conditions (Fuenzalida, 1951; Franz, 1966; Paskoff, 1970; Flores, 1983; Veit, 1996). The strong development of the Btb-horizons may in parts be favoured by high potassium values (Table 2). In many places of the Norte Chico, they may be classified as Solonetz or Natrargids (Luzio, 1986). The deeply reaching dry cracks and polygons in the Btb-horizon at La Serena may be explained by wetting-drying periods and the relatively high clay content. They indicate the sharp contrast of relatively wet conditions during the formation of the Btb and the following dry environment. It is not possible to deduce palaeoprecipitation values during the formation of the Btbs, because many factors may have played a role. The major problem is the influence of palaeoclimate versus time for soil formation (Schaetzl and Anderson, 2009). Could the well developed Btb-horizons reflect a very long stable time period (several $10x10^4$ years) with semiarid conditions, or are they really the result of a wetter palaeoclimate? Looking at the chronological data (Fig. 8), the Bw-horizons developed in a period of ca. 15 ka (Late Glacial/Holocene). It seems that 15 ka were not enough to produce Bt-horizons under modern climatic conditions, with 400–70 mm annual precipitation. At La Serena, Btb4 and Btb2 indicate a duration of soil development for ca. 10 ka. For Btb1 and Btb3 the time periods of soil formation cannot be fixed with a similar accuracy. However, in analogy to Btb4 and Btb2, a wetter climate seems probable. All soils (the modern Bws as well as the old Bbts) reflect long-lasting stable landscape conditions with a relatively dense vegetation cover, in contrast to the periods of sand accumulation.

Besides climate, wind speed and varying sediment supply through sea-level changes or river activity may have played a role in the alternating periods of soil development and sand accumulation (Pye, 1982; Pye and Tsoar, 1990; Clapperton, 1993; Lancaster, 1995; Stokes et al., 1997, 1998; Radies et al., 2004; Chase and Thomas, 2006a,b).Today, wind speed of 6.5–7.5 m s^{-1} as the monthly mean along the Norte Chico is high enough to transport fine to medium sand, as dominates in the palaeodunes (Table 2). Increasing wind speed would not greatly change, and only intensify, sand transport in areas where dune formation already takes place today, such as north of river mouths. However, this would not supply sand to other areas along the coast. Additionally, the coarse sand fraction in the aeolian record of the paleodunes is consistantly lacking. Looking at the granulometry, there is no indication of a changing wind regime during accumulation that would allow for the transport of coarse sand. The same holds true for intensified sand accumulation by rivers, probably related to climate change in the Andes, far away from the coast. More sand accumulation would intensify aeolian dynamics, but only in the same places where it occurs today.

Changing sea-level theoretically might have had a major influence on dune formation (e.g., Radies et al., 2004). The continental shelf north of 33°S is narrow, rarely exceeding a width of more than 5 km (Marchant et al., 2007). The shelf edge to the deep-sea trench is situated at a depth of −120 to −150 m. Therefore, during the LGM, a great part of the shelf was probably exposed to winds, due to global sea level lowering. However, the generally lower sea-level during the glacial periods

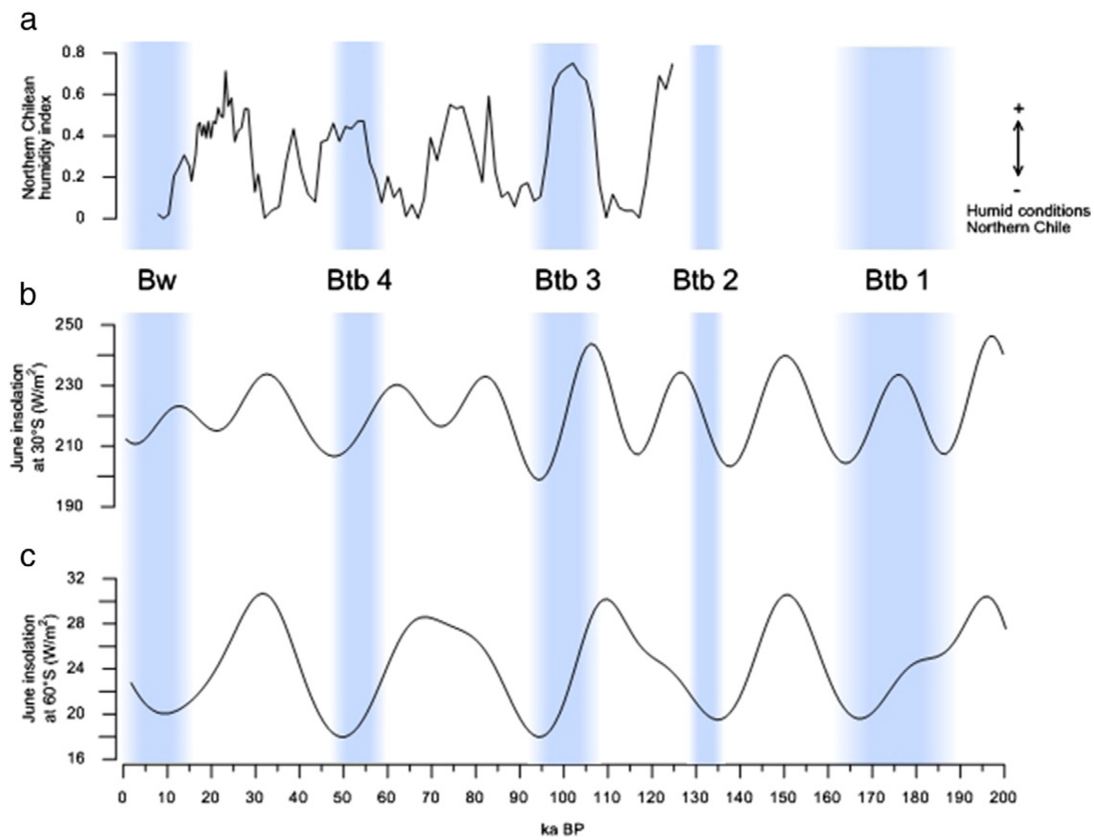

Fig. 9. Palaeo-Geoecology of the Norte Chico for the past two glacial cycles; a) humidity index derived from a marine core off Northern Chile at 27°S (GeoB3375-1, Stuut and Lamy, 2004); b) reconstructed winter insolation (June) at 30°S; c) reconstructed winter insolation (June) at 60°S (insolation values after Berger and Loutre, 1991).

cannot explain the cyclicity of the record (Fig. 9). In spite of lower sea-levels, several periods with landscape stability and soil development occurred. A dry climate with sparse vegetation cover on the different marine terraces along the coast would have allowed overall sand transport and dune formation, no matter where the coastline was located.

The only other existing long palaeoclimatic record from the region is the marine record of Stuut and Lamy (2004; Fig. 9a), at about 27°S. Their interpretation of periods with increased humidity in the Norte Chico in parts coincides with our palaeosol record. This applies for the periods around 50 ka, 100 ka and probably 130 ka. In other words, all relatively wet periods identified by palaeosols (Btbs) in this paper coincide with periods of increased humidiy as indicated by the marine record. However, the wetter periods in the marine record at about 25 ka (LGM) and 75 ka do not have an equivalent record in our sequences.

Two possible scenarios could explain this discrepancy: firstly, it could simply reflect a lack of conservation of these two periods in the palaeosol record. As a matter of fact, none of the investigated sections is complete by reflecting all four Btb-horizons. Additionally, the LGM with the maximal lowering of sea levels might reflect a special situation. It cannot be excluded, that intensified aeolian dynamics on the dry shelf

Table 2
Analytical characteristics of Bw-, Bt- and C-horizons. Values indicate the range between the 3 locations La Serena, Los Vilos and Las Ventanas. (x = rare; xx = frequent; xxx = dominant).

Grain size (mm; in %)							
Horizon	0.63–2.0	0.2–0.63	0.063–0.2	0.02–0.063	0.0063–0.02	0.002–0.0063	<0.002
Bw	0	28–37	45–51	5–10	0–1	0–1	0–1
fBt's	0	26–35	30–49	3–10	0–2	0–1	11–25
C	0	32–36	54–59	6–9	0–1	0–1	0–1
Horizon	pH ($CaCl_2$)	Fe_o (%)	Fe_d (%)	Na (%)	Kaol.	Illite	Inter-layered
Bw	6.4–6.6	0.04–0.06	0.7–1.0	2–5	x	xxx	-
fBt's	6.5–7.1	0.02–0.03	1.0–3.0	8–12	x	xx	xx
C	6.7–7.0	0.0	0.0	8–13	x	xx	xx

Heavy minerals						
Horizon	Augite	Epidote	Garnet	Amphibole	Titanite	Zircon
Bw	0–1	60–64	0–1	28–31	1–3	0–1
fBt's	0–3	60–67	0–2	27–35	1–2	0–1
C	0–4	60–63	0–1	28–33	1–2	0–1

overprinted wetter climatic conditions along the coast. Looking to soils further inland might help to answer this question in the future. For now, when looking to the periodicity of the palaeosols, missing paleosols in the profiles does not seem to be a very probable explanation. Secondly, the interpretation of Stuut and Lamy (2004) and Marchant et al. (2007) is mainly based on grain size variations in the marine sediments, allowing for the differentiation of aeolian dust (coarse, dry) and fluvial mud (fine, humid). Nevertheless, it should be considered that river discharge around their coring site at 27°S is today clearly dominant during austral summer (Gobierno de Chile, 2004; Houston, 2006). In the northern Atacama, these peaks in summer discharge may be attributed to tropical precipitation and a southward shift of the ITCZ. Therefore, increased amounts of fluvial sediments in the marine record at these latitudes might well reflect a major influence of the ITCZ on the Altiplano, and dry conditions in the Norte Chico. The same interpretation might also explain the maximum iron content of the LGM marine sediments at 30°S (Kaiser et al., 2008). According to these authors, the iron stems from volcanic rocks in the Andes and this could be explained by enhanced tropical summer rains. Therefore, the marine proxy might contain mixed tropical/extratropical information.

Other proxy data on the palaeoclimatic situation during the LGM for the SWW as well as for the Altiplano remain controversial. Whereas Baker et al. (2001) and Bobst et al. (2001) infer a humid LGM for the Altiplano and northern Chile, most authors report a dry LGM in that area, with increased moisture only during the Late Glacial and Early Holocene, as reflected in lake levels (Grosjean et al., 2001; Placzek et al., 2006; Servant and Fontes, 1978; Sylvestre et al., 1999), river discharge (Nester et al., 2007), rodent middens (Latorre et al., 2006), palaeowetlands (Betancourt et al., 2000; Latorre et al., 2002, 2003; Rech et al., 2002, 2003; Quade et al., 2008) and glacier advances (Kull et al., 2002; Zech et al., 2008).

For Central Chile and the SWW, overall humid conditions and a northward shift of the SWW during the LGM have been inferred from palynological studies in the Chilean Lake district (Heusser, 1983, 1989). Contrastingly, Markgraf (1989) concluded dry conditions and a southward shift of the SWW during the LGM in the same area. In central Chile, the water levels of Laguna Tagua-Tagua (34°30′) were highest during the LGM and prior to 42 ka (Valero-Garcés et al., 2005). Glacial records in the southern central Andes show major high stands prior to the LGM (Denton et al., 1999; Lowell et al., 1995; Zech et al., 2008, 2011). During the LGM, marine sedimentary records at 33°S and 41°S suggest SSTs of about 12 °C and 9 °C lower than today (Lamy et al., 2002, 2004). Antarctic sea ice and the ACC were in a northward position during the LGM (Ho et al., 2012). Antarctic cooling has been interpreted as leading to a steepened pressure gradient and a strengthening or southward displacement of the SPA (Garreaud and Falvey, 2009; Kaiser et al., 2008), which should result in drier conditions in the Norte Chico. The core zone of the SWW was probably intensified due to the steepened temperature gradient, but the northern limit did not change its position (Lamy et al., 2010).

All palaeosols appear to correlate with periods of low austral winter insolation at 60°S (Fig. 9). Therefore, increased sea ice around Antarctica could have acted like a "pushing factor" for the SWW during winter as it does today, when the area covered by sea ice is about four times larger than during summer conditions (16 million km^2 versus 4 million km^2; Kidston et al., 2011). Obliquity and Antarctic sea ice as a main influencing factor for the position of the SWW has also been discussed for South Africa (Stuut and Lamy, 2004). As a Holocene analogue increased humidity in the Norte Chico is documented after 6–4 ka, showing stronger influence of the SWW, expanding sea ice around Antarctica, decreasing SSTs (Lamy et al., 2002; Divine et al., 2010), and leading to glacier advances and increased river discharges in the Andes of the Norte Chico (Veit, 1996; Grosjean et al., 1998).

According to present day conditions, the intensity and position of the SPA acts as a "blocking factor" for the SWW (Fig. 2). In Fig. 9 the winter insolation at 30°S, which governs the medium position of the SPA, is plotted, reflecting the precession cycle. All the soil forming periods coincide with low insolation values, which is plausible, because this leads to low intensities of the SPA and the SWW may penetrate further north. Obviously, not every insolation minimum at 30°S is accompanied by increased influence of the SWW. This might show the important role of the obliquity cycle and Antarctic sea ice, which push the SWW northwards or not. Insolation at 30°S alone is not sufficient as an explanation for the observed changes.

7. Conclusions

Aeolian sands with interbedded palaeosols along the coast of the semiarid "Norte Chico" in Central Chile reflect environmental changes during the last 190 ka. Palaeosols formed during periods of long-lasting landscape stability with a relatively dense vegetation cover, whereas the accumulation of sands reflects periods with increased morphodynamics. These environmental changes can be mainly attributed to climate oscillations and changes in humidity. As is the case today, increased moisture input to the coastal region of the Norte Chico was only possible by increased influence of the Southern Westerly Winds (SWW).

Based on 16 PostIR225 luminescence dates, the variable influence of the SWW followed a periodicity, reflecting the obliquity cycle and insolation values at high southern latitudes. Today, the position and intensity of the SWW and the amount of precipitation in the Norte Chico is controlled by the strength and position of the South Pacific Anticyclone (SPA) in the north, and the sea ice extend around Antarctica in the south. In analogy to modern conditions, the variability of the SWW during the past two glacial cycles may be interpreted as being strongly influenced by Antarctic sea ice extend as a pushing factor, and the SPA as a blocking factor.

Acknowledgements

Funding was provided by the Geographical Institute of Bern. Gamma spectrometric measurements were carried out by Sönke Szidat, Department of Chemistry & Biochemistry, University of Bern, which is kindly acknowledged here. We thank Sally Lowick for her support with regard to carrying out the luminescence measurements at the Institute of Geological Sciences, University of Bern. Dylan Ward, Jason Rech and an unnamed reviewer helped to improve the paper considerably.

References

Aceituno, P., 1988. On the functioning of the southern oscillation in the Southern American sector. Part I. Surface climate. Mon. Weather Rev. 116, 505–524.
Armesto, J.J., Arroyo, M.T.K., Hinojosa, L.F., 2007. The Mediterranean environment of central Chile. In: Veblen, T.T., Young, K.R., Orme, A.R. (Eds.), The physical geography of South America. Oxford Univ. Press, pp. 184–199.
Auclair, M., Lamothe, M., Huot, S., 2003. Measurement of anomalous fading for feldspar IRSL using SAR. Radiat. Meas. 37, 487–492.
Baker, P.A., Seltzer, G.O., Fritz, S.C., Dunbar, R.B., Grove, M.J., Tapia, P.M., Cross, S.L., Rowe, H.D., Broda, J.P., 2001. The history of South American tropical precipitation for the past 25,000 years. Science 291, 640–643.
Berger, A., Loutre, M.F., 1991. Insolation values for the climate of the last 10 million of years. Quat. Sci. Rev. 10, 297–317.
Betancourt, J.L., Latorre, C., Rech, J.A., Quade, J., Rylander, K.A., 2000. A 22'000-year record of monsoonal precipitation from northern Chile's Atacama desert. Science 289, 1542–1546.
Blair, M.W., Yukihara, E.G., McKeever, S.W.S., 2005. Experiences with single-aliquot OSL procedures using coarse-grain feldspars. Radiat. Meas. 39, 361–374.
Blume, H.-P., 1985. Klimabezogene Deutung rezenter und reliktischer Eigenschaften von Wüstenböden. Geomethodica 10, 91–121.
Bobst, A.L., Lowenstein, T.K., Jordan, T.E., Godfrey, L.V., Ku, T.-L., Luo, S., 2001. A 106 ka paleoclimate record from drill core of the Salar de Atacama, northern Chile. Palaeogeogr. Palaeoclimatol. Palaeoecol. 173, 21–42.
Buylaert, J.P., Murray, A.S., Thomsen, K.J., Jain, M., 2009. Testing the potential of an elevated temperature IRSL signal from K-feldspar. Radiat. Meas. 44, 560–565.
Buylaert, J.-P., Jain, M., Murray, A.S., Thomsen, K.J., Thiel, C., Sohbati, R., 2012. A robust feldspar luminescence dating method for Middle and Late Pleistocene sediments. Boreas 41, 435–445.

Caviedes, C.N., 1990. Rainfall variations, snowline depression and vegetational shifts in Chile during the Pleistocene. Climate Change 16, 99–114.
Cerveny, R.S., 1998. Present climates of South America. In: Hobbs, J.E., Lindesay, J.A., Bridgman, H.A. (Eds.), Climates of the southern continents: Present, past and future. Wiley and Sons, Chichester, pp. 107–135.
Chase, B.M., Thomas, D.S.G., 2006a. Late Quaternary dune accumulation along the western margin of South Africa: distinguishing forcing mechanisms through the analysis of migratory dune forms. Earth Planet. Sci. Lett. 251, 318–333.
Chase, B.M., Thomas, D.S.G., 2006b. Multiphase late Quaternary aeolian sediment accumulation in western South Africa: Timing and relationship to palaeoclimatic changes inferred from the marine record. Quat. Int. 66, 29–41.
Clapperton, C., 1993. Quaternary geology and geomorphology of South America. Elsevier, Amsterdam (779 pp.).
Denton, G.H., Lowell, T.V., Heusser, C.J., Schlüchter, C., Andersen, B.G., Heusser, L.E., Moreno, P.I., Marchant, D.R., 1999. Geomorphology, stratigraphy, and radiocarbon chronology of Llanquihue drift in the area of the southern Lake District, Seno Reloncaví, and Isla Grand de Chiloé, Chile. Geogr. Ann. 81A, 167–229.
Divine, D.V., Koc, N., Isaksson, E., Nielsen, S., Crosta, X., Godtliebsen, F., 2010. Holocene Antarctic climate variability from ice and marine sediment cores: Insights on ocean-atmosphere interaction. Quat. Sci. Rev. 29, 303–312.
Flores, R., 1983. Pedogénesis de cuatro Aridisols en el secano costero de la IV. Región de Chile. Univ. de Chile, Fac. Ciencias Agrarias, Veterinarias y Forestales, Santiago (61 pp.).
Franz, H., 1966. Quartäre Sedimente und Böden in Chile und Argentinien sowie ihre Bedeutung für die biogeographische Forschung. Rev. Écol. Biol. Sol 3 (3), 355–379.
Fuenzalida, H., 1951. Pedálferes en el Norte Chico y sus relaciones con relíctos vegetacionales. Inf. Geogr. 3–4, 62–64.
Garreaud, R.D., Falvey, M., 2009. The coastal winds off western subtropical South America in future climate scenarios. Int. J. Climatol. 29, 543–554.
Gilli, A., Ariztegui, D., Anselmetti, F.S., McKenzie, J.A., Markgraf, V., Hajdas, I., McCulloch, R.D., 2005. Mid-Holocene strengthening of the Southern Westerlies in South America - Sedimentological evidences from Lago Cardiel, Argentina (49°S). Global Planet. Chang. 49, 75–93.
Gobierno de Chile, 2004. Cuenca del Río Copiapó. Ministerio de Obras Publicas, Dirección general de Aquas, Santiago (122 pp.).
Grosjean, M., Geyh, M.A., Messerli, B., Schreier, H., Veit, H., 1998. A late Holocene (<2600 BP) glacial advance in the south-central Andes (29 °S), northern Chile. The Holocene 8, 473–479.
Grosjean, M., Van Leeuwen, J.F.N., Van der Knaap, W.O., Geyh, M.A., Ammann, B., Tanner, W., Messerli, B., Veit, H., 2001. A 22,000 ^{14}C year BP sediment and pollen record of climate change from Laguna Miscanti (23°S), northern Chile. Global Planet. Chang. 28, 35–51.
Herm, D., Paskoff, R., 1967. Vorschlag zur Gliederung des marinen Quartärs in Nord- und Mittel-Chile. N. Jb. Geol. Paläont. Mh. 10, 577–588.
Heusser, C.J., 1983. Quaternary pollen record from Laguna de Tagua Tagua, Chile. Science 219, 1429–1432.
Heusser, C.J., 1989. Southern Westerlies during the Last Glacial Maximum. Quat. Res. 31, 423–425.
Hijmans, R.J., Cameron, S.E., Parra, J.L., Jones, P.G., Jarvis, A., 2005. Very high resolution interpolated climate surfaces for global land areas. Int. J. Climatol. 25, 1965–1978.
Ho, S.L., Mollenhauer, G., Lamy, F., Martínez-Garcia, A., Mohtadi, M., Gersonde, R., Hebbeln, D., Nunez-Ricardo, S., Rosell-Melé, A., Tiedemann, R., 2012. Sea surface temperature variability in the Pacific sector of the Southern Ocean over the past 700 ka. Paleoceanography 27, PA4202. http://dx.doi.org/10.1029/2012PA002317.
Hodgson, D.A., Sime, L.C., 2010. Southern westerlies and CO_2. Nat. Geosci. 3, 666–667.
Houston, J., 2006. Variability of precipitation in the Atacama Desert: its auses and hydrological impact. Int. J. Climatol. 26, 2181–2198.
Huntley, D.J., Baril, M.R., 1997. The K content of the K-feldspars beeing measured in optical dating or in thermoluminescence dating. Ancient TL 15, 11–14.
Huntley, D.J., Lamothe, M., 2001. Ubiquity of anomalous fading in K-feldspars and the measurement and correction for it in optical dating. Can. J. Earth Sci. 38, 1093–1106.
Jenny, B., Valero-Garcés, B.L., Villa-Martinez, R., Urrutia, R., Geyh, M., Veit, H., 2002. Early to Mid-Holocene aridity in central Chile and the Southern Westerlies: The Laguna Aculeo record (34 °S). Quat. Res. 58, 160–170.
Jenny, B., Wilhelm, D., Valero-Garcés, B.L., 2003. The Southern Westerlies in Central Chile: Holocene precipitation estimates based on a water balance model for Laguna Aculeo (33°50′S). Clim. Dyn. 20, 269–280.
Kaiser, J., Schefuss, E., Lamy, F., Mohtadi, M., Hebbeln, D., 2008. Glacial to Holocene changes in sea surface temperature and coastal vegetation in north central Chile: high *versus* low latitude forcing. Quat. Sci. Rev. 27, 2064–2075.
Karoly, D.J., 1989. Southern hemisphere circulation features associated with El Niño-southern oscillation events. J. Clim. 2, 1239–1252.
Kidston, J., Taschetto, A.S., Thompson, D.W.J., England, M.H., 2011. The influence of southern hemisphere sea-ice extent on the latitude of the mid-latitude jet stream. Geophys. Res. Lett. 38, L15804. http://dx.doi.org/10.1029/2011GL04056.
Kohfeld, K.E., Graham, R.M., de Boer, A.M., Sime, L.C., Wolff, E.W., Le Quéré, C., Bopp, L., 2013. Southern Hemisphere westerly wind changes during the Last Glacial Maximum: paleo-data synthesis. Quat. Sci. Rev. 68, 76–95.
Kulig, G., 2005. Erstellung einer Auswertesoftware zur Altersbestimmung mittels Lumineszenzverfahren. BSc thesis, Faculty of Mathematics and Informatics TU Freiberg, Germany (unpublished).
Kull, C., Grosjean, M., Veit, H., 2002. Modelling Modern and Late Pleistocene glacio-climatological conditions in the North Chilean Andes (29°S - 30°S). Climate Change 53, 359–381.
Lamy, F., Hebbeln, D., Röhl, U., Wefer, G., 2001. Holocene rainfall variability in southern Chile: A marine record of latitudinal shifts of the southern westerlies. Earth Planet. Sci. Lett. 185, 369–382.
Lamy, F., Rühlemann, C., Hebbeln, D., Wefer, G., 2002. High- and low-latitude climate control on the position of the southern Peru-Chile current during the Holocene. Paleoceanography 17, 1601–1610.
Lamy, F., Kaiser, J., Ninnemann, U., Hebbeln, D., Arz, H.W., Stoner, J., 2004. Antarctic Timing of Surface Water Changes off Chile and Patagonian Ice Sheet Response. Science 304, 1959–1962.
Lamy, F., Kilian, R., Arz, H.W., Francois, J.-P., Kaiser, J., Prange, M., Steinke, T., 2010. Holocene changes in the position and intensity of the southern westerly wind belt. Nat. Geosci. http://dx.doi.org/10.1038/NGEO959.
Lancaster, N., 1995. Geomorphology of desert dunes. Routledge, London (290 pp.).
Latorre, C., Betancourt, J.L., Rylander, K.A., Quade, J., 2002. Vegetation invasions into absolute desert: A 45'000 yr rodent midden record from the Calam-Salar de Atacama basins, northern Chile (lat 22°-24°S). Geol. Soc. Am. Bull. 114 (3), 349–366.
Latorre, C., Betancourt, J.L., Rylander, K.A., Quade, J., Matthei, O., 2003. A vegetation history from the arid prepuna of northern Chile (22-23°S) over the last 13,500 years. Palaeogeogr. Palaeoclimatol. Palaeoecol. 194, 223–246.
Latorre, C., Betancourt, J.L., Arroyo, M.T.K., 2006. Late Quarternary vegetation and climate history of the perennial river canyon in the Río Salado basin (22°S) of Northern Chile. Quat. Res. 65, 450–466.
Lowell, T.V., Heusser, C.J., Andersen, B.G., Moreno, P.I., Hauser, A., Heusser, L.E., Schlüchter, Ch., Marchant, D.R., Denton, G.H., 1995. Interhemispheric correlation of Late Pleistocene glacial events. Science 269, 1541–1549.
Lu, J., Chen, G., Frierson, D.M.W., 2010. The position of the midlatitude storm track and eddy-driven westerlies in aquaplanet AGCMs. J. Atmos. Sci. 67, 3984–4000.
Luzio, W., 1986. Genesis y clasificación de los suelos de regiones áridas y deserticas de Chile. Soc. Chil. Cienc. Suelo Bol. 5, 107–140.
Marchant, M., Cecioni, A., Figueroa, S., González, H., Giglio, S., Hebbeln, D., Kaiser, J., Lamy, F., Mohtadi, M., Pineda, V., Romero, O., 2007. Marine geology, oceanography and climate. In: Moreno, T., Gibbons, W. (Eds.), The geology of Chile. Geol. Soc. London, pp. 289–308.
Markgraf, V., 1989. Reply to C.J. Heusser's "Southern Westerlies during the Last Glacial Maximum". Quat. Res. 31, 426–432.
Markgraf, V., Dodson, J., Kershaw, A.P., McGlone, M.S., Nichollis, N., 1992. Evolution of late Pleistocene and Holocene climates in the circum-South Pacific land areas. Clim. Dyn. 6, 193–211.
Mayr, C., Wille, M., Haberzettl, T., Fey, M., Janssen, S., Lücke, A., Ohlendorf, C., Oliva, G., Schäbitz, F., Schlesaer, G.H., Zolitschka, B., 2007. Holocene variability of the Southern Hemisphere westerlies in Argentinean Patagonia (52°S). Quat. Sci. Rev. 26, 579–584.
Mehra, O.P., Jackson, M.L., 1960. Iron oxide removal from soils and clays by dithionit-citrate systems buffered with sodium bicarbonate. Clay Clay Miner. 7.
Moreno, P.I., Francois, J.P., Moy, C.M., Villa-Martínez, R., 2010. Covariability of the Southern Westerlies and atmospheric CO_2 during the Holocene. Geology 38, 727–730.
Nester, P.L., Gayó, E., Latorre, C., Jordan, T.E., Blanco, N., 2007. Perennial stream discharge in the hyperarid Atacama Desert of northern Chile during the latest Pleistocene. PNAS 50, 19724–19729.
Paskoff, R., 1970. Le Chili semi-aride. Biscaye Frères Publishers, Bordeaux (420 pp.).
Placzek, C., Quade, J., Patchett, P.J., 2006. Geochronology and stratigraphy of late Pleistocene lake cycles on the southern Bolivian Altiplano: implications for causes of tropical climate change. Geol. Soc. Am. Bull. 515–532.
Preusser, F., Kasper, H.U., 2001. Comparison of dose rate determination using high-resolution gamma spectrometry and inductively coupled plasma – mass spectrometry. Ancient TL 19, 19–23.
Preusser, F., Muru, M., Rosentau, A., 2014. Comparing different post-IR IRSL approaches for the dating of Holocene coastal foredunesfrom Ruhnu Island, Estonia. Geochronometria 41, 342–351.
Pye, K., 1982. Morphological development of coastal dunes in a humid tropical environment, Cape Bedford and Cape Flattery, North Queensland. Geogr. Ann. Ser. A 64, 213–227.
Pye, K., Tsoar, H., 1990. Aeolian sand and sand dunes. Unwin Hyman, London.
Quade, J., Rech, J.A., Betancourt, J.L., Latorre, C., Quade, B., Rylander, K.A., Fischer, T., 2008. Paleowetlands and regional climate change in the Central Atacama Desert, northern Chile. Quat. Res. 69, 343–360.
Radies, D., Preusser, F., Matter, A., Mange, M., 2004. Eustatic and climatic controls on the development of the Wahiba Sand Sea, Sultanate of Oman. Sedimentology 51, 1359–1385.
Radtke, U., 1989. Marine Terrassen und Korallenriffe – das Problem der quartären Meeresspiegelschwankungen erläutert an Fallstudien aus Chile, Argentinien und Barbados. Düsseldorfer Geographische Studien 27, (246 pp.).
Rahn, D.A., Garreaud, R.D., 2013. A synoptic climatology of the near-surface wind along the west coast of South America. Int. J. Climatol. http://dx.doi.org/10.1002/joc.3724.
Rech, J.A., Quade, J., Betancourt, J.L., 2002. Late Quaternary paleohydrology of the central Atacama Desert (22-24°S), Chile. Geol. Soc. Am. Bull. 114, 334–348.
Rech, J.A., Pigati, J.S., Quade, J., Betancourt, J.L., 2003. Re-evaluation of mid-Holocene deposits at Quebrada Puripica, northern Chile. Palaeogeogr. Palaeoclimatol. Palaeoecol. 194, 207–222.
Rojas, M., Moreno, P., Kageyama, M., Cruifix, M., Hewitt, C., Abe-Ouchi, A., Ohgaito, R., Brady, E.C., Hope, P., 2009. The Southern Westerlies during the last glacial maximum in PIMP2 simulations. Clim. Dyn. 32, 525–548.
Ruttland, J., Fuenzalida, H., 1991. Synoptic aspects of central Chile rainfall variability associated with the Southern Oscillation. Int. J. Climatol. 11, 63–76.
Saavedra, N., Müller, E.P., Foppiano, A.J., 2010. On the climatology of surface wind direction frequencies for the central Chilean coast. Aust. Meteorol. Oceanogr. J. 60, 103–112.
Schaetzl, R.J., Anderson, S., 2009. Soils. Genesis and geomorphology. Cambridge University Press, New York (817 pp.).

Schwertmann, U., 1964. Differenzierung der Eisenoxide des Bodens durch Extraktion mit Ammoniumoxalat-Lösung, Zeitschrift f. Pflanzenernährung, Düngung und Bodenkunde 105, 194–202.

Servant, M., Fontes, J.C., 1978. Les lacs quaternaires des hauts plateaux des Andes boliviennes. Premières interprétations paléoclimtaiques. Cah. Orstom Ser. Geol. 10 (1), 9–23.

Simmonds, T., Jacka, H., 1995. Relationship between the interannual variability of Antarctic sea-ice and the Southern Ocillation index. J. Clim. 8, 637–647.

Sohbati, R., Murray, A.S., Buylaert, J.P., Ortuño, M., Cunha, P.P., 2011. Luminescence dating of Pleistocene alluvial sediments affected by the Alhama de Murcia fault (southeastern Betics, Spain) – a comparison between OSL, IRSL and post-IR IRSL ages. Boreas 41, 250–262.

Spooner, N.A., 1994. The anomalous fading of infrared-stimulated luminescence from feldspars. Radiat. Meas. 23, 625–632.

Steffen, D., Preusser, F., Schlunegger, F., 2009. OSL quartz age underestimation due to unstable signal components. Quat. Geochronol. 4, 1975–1989.

Stokes, S., Thomas, D.S.G., Washington, R., 1997. Multiple episodes of aridity in southern Africa since the last interglacial period. Nature 388, 154–158.

Stokes, S.G., Haynes, D.S.G., Thomas, J.L., Horrocks, M., Higginson, Malifa, M., 1998. Punctuated aridity in southern Africa during the last glacial cycle: the chronology of linear dune construction in the northeastern Kalahari. Palaeogeogr. Palaeoclimatol. Palaeoecol. 137, 305–322.

Stuut, J.-B.W., Lamy, F., 2004. Climate variability at the southern boundaries of the Namib (southwestern Africa) and Atacama (northern Chile) coastal deserts during the last 120,000 yr. Quat. Res. 62, 301–309.

Stuut, J.-B.W., Marchant, M., Kaiser, J., Lamy, F., Mohtadi, M., Romero, O., Hebbeln, D., 2006. The late Quaternary paleoenvironment of Chile as seen from marine archives. Geograph. Helv. 61, 135–151.

Sylvestre, F., Servant, M., Servant-Vildary, S., Causse, C., Fournier, M., Ybert, J.-P., 1999. Lake-level chronology on the Southern Bolivian Altiplano (18°- 23°S) during Late-Glacial time and the Early Holocene. Quat. Res. 51, 54–66.

Thomsen, K.J., Murray, A.S., Jain, M., Bøtter-Jensen, L., 2008. Laboratory fading rates of various luminescence signals from feldspar-rich sediment extracts. Radiat. Meas. 43, 1474–1486.

Toggweiler, J.R., Russell, J.L., Carson, S.R., 2006. Midlatitude westerlies, atmospheric CO_2, and climate change during the ice ages. Palaeoceanography 21, PA2005. http://dx.doi.org/10.1029/2005PA001154.

Trauerstein, M., Lowick, S.E., Preusser, F., Schlunegger, F., 2014. Small aliquot and single grain IRSL and post-IR IRSL dating of fluvial and alluvial sediments from the Pativilca valley, Peru. Quat. Geochronol. 22, 163–174.

Valdes, P.J., 2000. South American palaeoclimate model simulations: how reliable are the models? J. Quat. Sci. 15, 357–368.

Valero-Garcés, B.L., Jenny, B., Rondanelli, M., Delgado-Huertas, A., Burns, S.J., Veit, H., Moreno, A., 2005. Paleohydrology of Laguna de Tagua Tagua (34°30′S) and moisture fluctuations in Central Chile for the last 46,000 years. J. Quat. Sci. 20, 625–641.

Veit, H., 1996. Southern Westerlies during the Holocene deduced from geomorphological and pedological studies in the Norte Chico, Northern Chile (27-33°S). Palaeogeogr. Palaeoclimatol. Palaeoecol. 123, 107–119.

Villagrán, C., 1990. Glacial climates and their effects on the history of the vegetation of Chile: A synthesis based on palynological evidence from Isla de Chiloé. Rev. Palaeobot. Palynol. 65, 17–24.

Villagrán, C., Armesto, J.J., 1993. Full and late glacial paleoenvironmental scenarios for the west coast of southern South America. In: Mooney, H.A., Fuentes, E.R., Kronberg, B.I. (Eds.), Earth system responses to global change: contrasts between North and South America. Academic Press, pp. 195–207.

Villagrán, C., Armesto, J.J., Hinojosa, L.F., Cuvertino, J., Pérez, C., Medina, C., 2004. El enigmático origen del bosque relicto de Fray Jorge. In: Squeo, F.A., Gutiérrez, J.R., Hernández, I.R. (Eds.), Historia Natural del Parque Nacional Bosque Fray Jorge, pp. 3–43.

Villa-Martínez, R., Villagrán, C., Jenny, B., 2003. The last 7500 cal yr B.P. of westerly rainfall in Central Chile inferred from a high-resolution pollen record from Laguna Aculeo (34°S). Quat. Res. 60, 284–293.

Wainer, I., Clauzet, G., Ledru, M.-P., Brady, E., Otto-Bliesner, B., 2005. Last Glacial Maximum in South America: palaeoclimate proxies and model results. Geophys. Res. Lett. 32, L08702. http://dx.doi.org/10.1029/2004GL021244.

Wintle, A.G., 1973. Anomalous fading of thermoluminescence in mineral samples. Nature 245, 143–144.

Wyrwoll, K.-H., Dong, B., Valdes, P., 2000. On the position of southern hemisphere westerlies at the Last Glacial Maximum: an outline of AGCM simulation results and evaluation of their implications. Quat. Sci. Rev. 19, 881–898.

Zech, R., Kull, C., Veit, H., 2006. Late Quarternary glacial history in the Encierro Valley, northern Chile (29°S), deduced from ^{10}Be surface exposure dating. Palaeogeogr. Palaeoclimatol. Palaeoecol. 234, 277–286.

Zech, R., Kull, C., Ilgner, J., Kubik, P., Veit, H., 2008. Timing of the Late Quaternary Glaciation in the Andes from ~15 to ~40°S. J. Quat. Sci. 23, 635–647.

Zech, R., Zech, J., Kull, C., Kubik, P.W., Veit, H., 2011. Early last glacial maximum in the southern Central Andes reveals northward shift of the westerlies at ~39 ka. Clim. Past 7, 41–46.